The representation of the South Tropical Atlantic teleconnection to the Indian Ocean in the AR4 coupled models

Rondrotiana Barimalala · Annalisa Bracco · Fred Kucharski

Abstract A series of recent papers showed that sea surface temperature (SST) anomalies in the south equatorial tropical Atlantic modulate the interannual variability of the African and Indian monsoon rainfall. Physically this teleconnection can be explained by a simple Gill-Matsuno mechanism. In this work, the output from five different models chosen within the CMIP3 (Coupled Model Intercomparison Project version 3) ensemble of coupled general circulation models (CGCMs) are analyzed to investigate how state-of-the-art CGCMs represent the impact of the South Tropical Atlantic (STA) SSTs on the Indian and African region. Using a correlation-regression technique, it is found that four out of the five models display a teleconnection between STA and Indian region which is generally weaker than in the observations but in agreement in the rainfall field pattern. This teleconnection is also noticeable in the ensemble mean of the five models. Over Africa, however, the significant changes in rainfall displayed in the observation are properly caught by only one of the CGCMs. Additionally, none of the models reproduces the symmetric upper-level wind response around the Equator seen over the Indian Ocean in the observations and all have significant biases also in the surface pressure field

response to the tropical Atlantic SSTs. Nonetheless the STA response, particularly over the southern hemisphere, is indicative of the Gill-Matsuno-type mechanism identified in previous studies using idealized experiments with atmospheric GCMs and observational data. With a suite of atmospheric-only GCM integrations it is shown that the differences in amplitude and pattern are not only due to the strong biases and reduced variabilities of the CGCMs over the tropical Atlantic but they are also caused by the different physical parameterizations used in models.

Keywords South Tropical Atlantic · African monsoon · Indian monsoon · Teleconnection · Coupled models

1 Introduction

Sea surface temperature anomalies (SSTa) in the tropical Atlantic influence interannual rainfall variability in the immediate surrounding regions, Africa and the Caribbean (Nobre and Shukla 1996; Janicot et al. 1998; Vizy and Cook 2001; Giannini et al. 2003; Shanahan et al. 2009). In response to a warming of the SST in the Gulf of Guinea, a low level convergent flow is observed in the nearby coastal areas. Such a flow brings moist air and thus increased precipitation over land. Recently Kucharski et al. (2007, 2008) and Losada et al. (2010) have found that in boreal summer the influence of the Atlantic SSTa south of the Equator extends further to the east, to the Indian peninsula. The physical mechanism by which heating anomalies in the Gulf of Guinea interconnect to Africa and the Indian ocean basin has been investigated by Kucharski et al. (2009) analyzing reanalysis data and with idealized atmospheric general circulation model (AGCM) experiments. The authors found that the atmosphere responds to an anomaly localized in the

R. Barimalala (✉) · F. Kucharski
Abdus Salam International Centre for Theoretical Physics,
Earth System Physics Section, Strada Costiera 11,
34014 Trieste, Italy
e-mail: rbarimal@ictp.it

F. Kucharski
e-mail: kucharsk@ictp.it

R. Barimalala · A. Bracco
EAS, Georgia Institute of Technology,
311 Ferst Drive, Atlanta, GA 30332, USA
e-mail: abracco@gatech.edu

south tropical Atlantic developing a Gill-Matsuno-type (Gill 1980) quadrupole in the eddy streamfunction with Kelvin and Rossby waves transporting the signal respectively to the east and to the west. The response to a warm (cold) SST anomaly in the tropical Atlantic consists of rising motion, an upper-level divergence (convergence) and a velocity potential minimum (maximum) in the equatorial Atlantic/African region. The compensating upper-level convergence (divergence) is located in the central-western Pacific and causes a maximum (minimum) in velocity potential there. The response is baroclinic with opposite anomalies at low levels. In the gradient of the upper-level velocity potential anomalies a pair of upper-level cyclones (anticyclones) develops in the subtropical regions at about 20°–30° both north and south of the Equator because of Sverdrup balance (e.g. Hoskins and Rodwell 2001; Chen 2003; Kucharski et al. 2010). At low-levels, a pair of anticyclones (cyclones) forms due to the same mechanism, leading to a high (low) surface pressure anomaly over India that triggers in turn an anomalous low level divergence (convergence) and a decrease (increase) of rainfall. Further, at upper levels, a warm (cold) tropical Atlantic SST anomaly leads to westerly (easterly) wind anomalies in the Indian Ocean region. At low levels, on the other hand, the Somali jet is weakened (strengthened). Figure 1 presents a schematic that summarizes the salient features of this mechanism for a positive south tropical Atlantic SST anomaly.

The response over the Indian basin projects largely onto the time-mean Indian monsoon circulation, and a tropical Atlantic warming (cooling) weakens (strengthens) the time-mean Walker circulation. Nonlinear interactions with the mean monsoon circulation cause a further enforcement of the Kelvin-wave response. Xie et al. (2009) also proposed a similar mechanism, called "Ekman Induced Kelvin wave divergence", to physically describe the influence of

the Indian Ocean SST on the subtropical western Pacific precipitation. As shown in Kucharski et al. (2007, 2008), the remotely forced response of the atmospheric circulation over the Indian basin to the south tropical Atlantic SST modulates the stronger and quasi-linear El Niño Southern Oscillation (ENSO)—Indian Summer monsoon relationship, according to which a weaker than normal monsoon precedes peak El Niño conditions and vice versa during summers preceding La Niña events (e.g. Turner et al. 2007). The tropical Atlantic SST variability represents therefore a potentially predictable contribution of the Indian Monsoon interannual variability.

In this paper we analyze how different coupled GCMs represent the specific impact of SST changes in the south tropical Atlantic on the African and Indian rainfall. State-of-the-art GCMs have been showed to vary widely in their ability to reproduce rainfall climatology and variability in West Africa and South Asia (e.g. Philippon et al. 2010; Xue et al. 2010; Joly and Voldoire 2009, 2010 for West Africa and Annamalai et al. (2007), Kim et al. (2008) for the South Asian region). In particular, Joly and Voldoire (2010) noted the difficulties of CMIP3 (Coupled Model Intercomparison Project version 3) models to reproduce the sea surface temperature climatology and variability in the Gulf of Guinea region and their influence on the West African Monsoon, confirming that the tropical Atlantic is a region where coupled models have very strong biases (Stockdale et al. 2006; Richter and Xie 2008). With the hope of identifying the sources for the model biases, we investigate the output of five different models selected from the AR4 coupled GCMs integrations for the XX century by using simple correlation-regression techniques. Only the atmospheric data are used in all the analysis as we focus on the atmospheric response of the south tropical Atlantic variability.

Fig. 1 Schematic of the mechanism of the tropical Atlantic SST teleconnection for a positive SST and therefore heating anomaly showing its influence on the global climate. See text for details
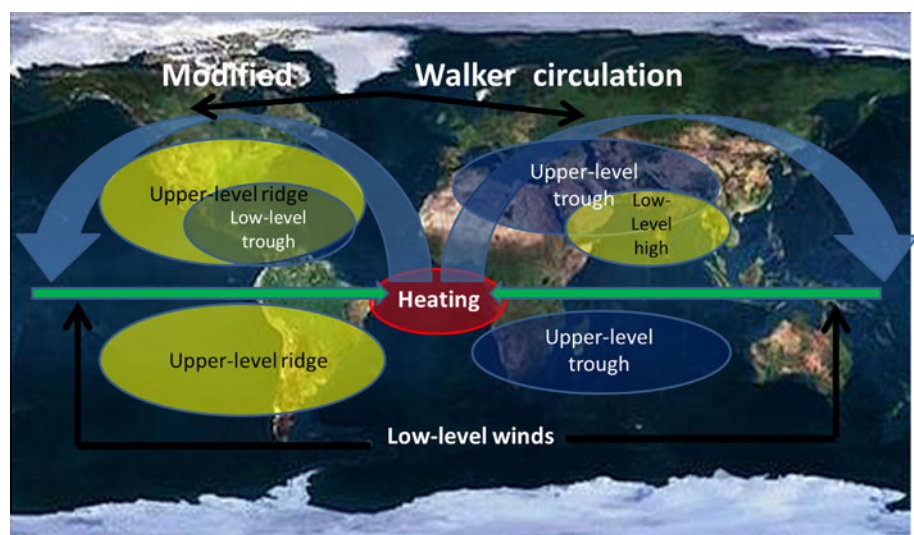
We find that four out of the five models analyzed are capable of reproducing correctly the rainfall response over India and the surface pressure and the high-level wind signals are consistent with a Gill-Matsuno type response as in the idealized AGCM runs in Kucharski et al. (2009), particularly in the southern hemisphere. The rainfall response over Africa, on the other hand, is barely caught by the models except for one that shows a strong precipitation anomaly over the Sahelian region. The role of the SST bias in the coupled models in the south tropical Atlantic is further investigated with a series of AGCM-only runs.

In Sect. 2 we introduce the observational and model data used in this study. Results follow in Sect. 3. Section 4 contains summary and conclusions.

2 Observational evidence and models description

In this study, we adopt the HadISST reanalysis (Rayner et al. 2003) as proxy for observed SST; CMAP (Center Merged Analysis of Precipitation; Xie and Arkin 1997), GPCP (Global Precipitation Climatology Project; Adler et al. 2003), CRU (Climate Research Unit; New et al. 1999), and Aphrodite (Asian Precipitation—Highly-Resolved Observational Data Integration Towards Evaluation of the Water Resources; Xie et al. 2007) data as observed precipitation; HadSLP2 (Hadley Center sea level pressure dataset 2; Allan and Ansell 2006) as surface pressure datasets; and NCEP/NCAR (National Centers for Environmental Prediction/National Center for Atmospheric research; Kalnay et al. 1996) reanalysis as proxy for observed winds and surface pressure. All analysis are performed over the 1950–2000 period, unless otherwise stated. The South Tropical Atlantic (STA) index used in our analysis is defined as the negative area average of the SST anomalies in the STA region (30°W—10°E and 20°S–0°) as in Enfield et al. (1999).

2.1 Global South Tropical Atlantic teleconnections in observations

Before analyzing the model outputs, we briefly review the current knowledge of the teleconnections of the South Tropical Atlantic SST anomalies to remote regions, with special emphasis on the Indian Ocean region. Focusing on the tropics, the interference of SST variabilities from regions other than the South Tropical Atlantic and in particular from the Pacific on the tropical Atlantic has to be verified. Indeed, the SST variability in the tropical Atlantic has been often viewed as linked to ENSO (Zebiak 1993; Latif and Grötzner 2000; Handoh et al. 2006; Saravanan and Chang 1999, 2000; Chang et al. 2006). Several works, however, have pointed out that the variability in the Tropical Atlantic south of the equator results from an

independent mode, intrinsic to the Atlantic Ocean (Enfield and Mayer 1997; Huang et al. 2004; Hu and Huang 2007).

To test the existence of an ENSO-STA relation in the HadISST dataset we perform a lead-lag correlation analysis between the STA and NIÑO34 (area averaged of SST anomaly within 190°E–240°E, 5°S–5°N) indices over the period 1950–2000 focusing on June to September (JJAS). The STA index is fixed at JJAS, and the 4-month averaged NIÑO34 index is shifted. Therefore, positive lags are indicative of the STA index leading NIÑO34 and vice versa for negative lags.

The HadISST data-set displays no statistically significant correlation between the two indices for a lead-lag of 7 months or less (Fig. 2a, shaded area). A barely statistically significant correlation of 0.3 is achieved for the NIÑO34 index preceding the STA anomalies by 8 months.

Figure 2b shows the global SST regression map onto the STA index in the HadISST data for 1950–2000. Shaded areas in this and following regression maps represent the regions where the anomalies are statistically significant at the 10% level according to t test based on the temporal standard deviation of a field at every grid-point and assuming 50 degrees of freedom. Only a weak signal is seen in the Pacific, centered in the warm pool. This confirms the independence between most the Pacific and the south tropical Atlantic. On the other hand, a statistically significant negative signal is seen in the Indian Ocean. This is in agreement with a recent analysis by Wang et al. (2009) showing that during the 1950–2000 period warm (cold) SST anomalies in the STA region induced low level easterly (westerly) wind anomalies in the western tropical Indian Ocean that in turn can affect locally the SST.

In some of the CMIP3 coupled models that we analyze the teleconnections between the ENSO region and the adjacent basins are too strong. With the goal of isolating the teleconnection between the STA region and the African continent and Indian basin, in the following all regressions are computed removing the linear effect of ENSO on the tropical Atlantic. This dependence is instantaneously deducted from the STA index following the procedure adopted in Kucharski et al. (2008) by defining

$$SST_{res}(t) = SST(t) - SST_{ENSO}(t) \qquad (1)$$

where

$$SST_{ENSO}(t) = b\,NI\tilde{N}O34(t) \qquad (2)$$

and b is a constant determined by least square fitting. The reader should bear in mind that time-lagged and non-linear teleconnections with ENSO cannot be excluded using this linear relationship. While this operation does not change in any significant way the regression maps for observed quantities, it does affect few of the climate model outputs, as we will further discuss below.

(a)

(b)

(c)

(d)

(e)

(f)

(g)

(h)

(i)

(j)
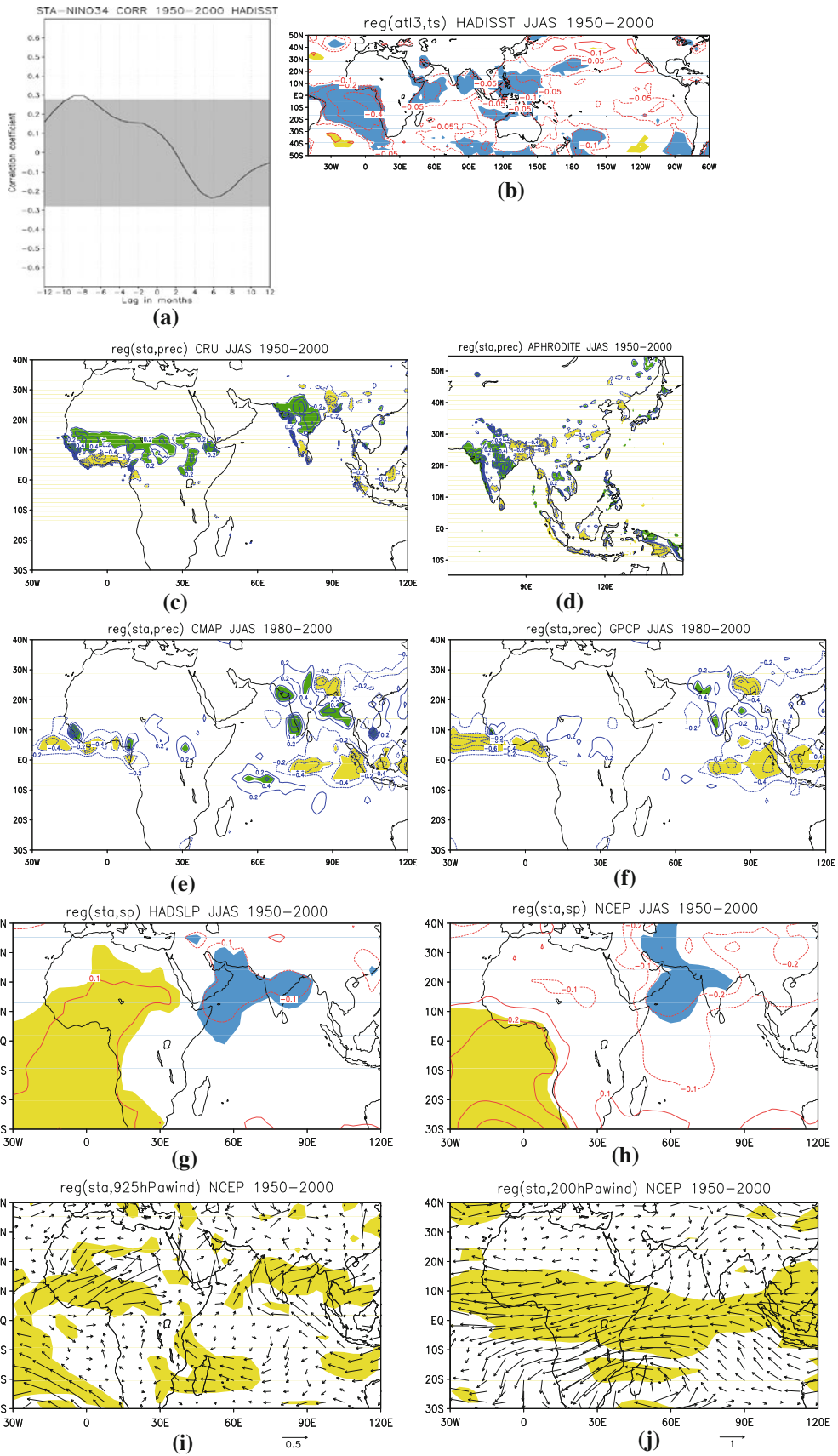
◄ **Fig. 2** **a** Plot of the lagged correlation coefficient between the JJAS STA index and the (lagged) 4-months average NIÑO34 index for the HadISST data set. NIÑO34 is leading STA for negative lags, and vice versa positive lags. *White areas* indicate where the correlation is statistically significant at the 5% level; the shaded ones where the correlations is not significant. **b** SST regression onto the STA index using HadISST. Units are *K*. **c–f** Precipitation regression map onto the STA index using CRU, APHRODITE, CMAP, GPCP respectively. Units are mm day^{-1}. **g–h** Surface Pressure regression onto the STA index for HADSLP and NCEP-NCAR reanalysis, respectively. Units are hPa. **i** Near Surface and **j** 200 hPa wind regression onto the STA index using NCEP-NCAR reanalysis. Units are m s^{-1}. All analysis are performed over the 1950–2000 period. Shaded areas in the regression maps indicate anomalies statistically significant at the 10% level according to a *t* test

In Fig. 2c–f focus on the precipitation rainfall response to STA anomalies. Figure 2c shows the regression of CRU rainfall over land onto the STA index over the whole 1950–2000 interval, Fig. 2d shows the Aphrodite data regression for 1951–2000 (this data is only available eastward of 60°E and over land). In Fig. 2e, f we display the regressions calculated using CMAP and GPCP data for 1980–2000, respectively. For those last two maps the statistical significance is calculated assuming 20 degrees of freedom. The common response to negative SST anomalies in the STA region in Fig. 2c, e and f is a decrease in precipitation over the Gulf of Guinea coast, an increase over the Sahel and India and a decrease in the equatorial Indian Ocean (not seen in the CRU being the data available only over land). Aphrodite data (Fig. 2d)—available over land and limited to the Asian continent—also shows an increase of rainfall over India.

The intensity of the response in the Sahel, however, differs between CRU and CMAP/GPCP, with CRU showing a strong increase, whereas CMAP and GPCP data display a weaker signal. Also over India the precipitation response in CMAP and GPCP at first glance appears somewhat reduced with respect to CRU and Aphrodite. The discrepancy over the Sahel can be explained considering that in the 1980–2000 period the STA and the Nino3.4 indices display a statistically significant instantaneous negative correlation (e.g. Kucharski et al. 2007; Rodriguez-Fonseca et al. 2010; Joly and Voldoire 2010). Once this is linearly removed following the procedure outlined above, the STA anomaly in SSTs is reduced in amplitude by about 1/3 compared to the whole 1950–2000 record (not shown). Such a reduction impacts the intensity of the rainfall response over the nearby Africa. The Indian basin is less sensitive to the amplitude of the STA anomalies compared to African continent and the apparent discrepancies between the data-sets can be understood by accounting for the shorter record of CMAP and GPCP, and therefore the limited statistical significance of the regression maps, and the different spatial resolution of the data-sets.

The STA influence on the Sahelian and Indian rainfall have been reproduced by idealized atmospheric general circulation models (AGCMs) (Vizy and Cook 2001; Giannini et al. 2003; Kucharski et al. 2007, 2008). It has been explained by a simple Gill-Matsuno-type mechanism (Kucharski et al. 2009) with the main heat source for the response being located near the equator, in the 0°–10°S band, although the STA anomaly extends further to the south. The reason is that the regions south of 10°S are too cold to produce large heating and convective precipitation anomalies. This is consistent with the rainfall responses near the equator over the Atlantic and Gulf of Guinea regions seen in the CMAP and GPCP data (see Fig. 2e, f).

Figure 2g and h show the surface pressure (SP) response to STA anomalies using HadSLP2 and NCEP-NCAR reanalysis data respectively. In both data-sets a negative SP anomaly is centered between the eastern portion of the Arabian peninsula and north and central India. In correspondence to the center of the anomaly a cyclone develops at low levels over the western part of the northern Indian Ocean (Fig. 2i) and brings a moist south-westerly flow over the Indian subcontinent, inducing the increase in precipitation. The response at higher level is baroclinic and of opposite sign in the wind field (Fig. 2j)[1] An equatorial easterly wind is accompanied by a pair of anticyclones in the southern and northern subtropics at about 50°E, 25°S and 50°E, 30°N. This is again consistent with the Gill-Matsuno mechanism and is in agreement with the upper-level velocity potential and streamfunction responses shown in Kucharski et al. (2009) in AGCM-only integrations.

We verified that, notwithstanding the limited statistical significance, all regressions for the CRU and re-analysis show similar patterns in the Indian region if the period 1980–2000, common to CMAP and GPCP data, is used (not shown).

2.2 Models

The goal of this study is to analyze how the STA teleconnection to the Indian Ocean is reproduced by state-of-the-art CGCMs. To this end we chose five models participating in the CMIP3 ensemble for the XX century (Table 1). We focus on the models with the most realistic monsoon climatology according to the analysis in Annamalai et al. (2007). Those models are the GFDL-CM2.1, of which there are three ensemble members, the MPI-ECHAM5 model (3 members), the MRI (5 members), the HadCM3 from the UK Met Office (1 member only) and the NCAR-PCM1 model (4 members). Only

---

[1] The statistical significance for all wind vector maps is based on a *t* test using the standard deviation of the wind speed.

Table 1 List of models analyzed in this study

Model	# of Members	Resolution	References
GFDL-CM2.1	3	2.5° × 2°L24	Delworth et al. (2006)
MPI-ECHAM5	3	T63L31	Jungclaus et al. (2006)
MRI	5	T42	Yukimoto et al. (2001)
UKMO-HadCM3	1	3.75° × 2.5°L19	Gordon et al. (2000)
NCAR-PCM1	4	T42L18	Washington et al. (2000)

Resolution and number of members for each ensemble are also indicated

the atmospheric monthly means have been utilized to investigate the STA atmospheric response. All the analysis extend to the 1950–2000 time period, focusing on the JJAS season. Ensemble means of individual models as well as the multi-model ensemble means are calculated by the arithmetic average of the model output.

To investigate the sources of errors in the CMIP3 CGCMs, we also perform a suite of sensitivity experiments using the ICTP AGCM (Molteni et al. 2003; Kucharski et al. 2006) which is based on a hydrostatic spectral dynamical core (Held and Suarez 1994), and uses the vorticity-divergence form described by Bourke (1974). The ICTP AGCM is configured with 8 vertical (sigma) levels and with a spectral truncation at total wavenumber T30. The model includes physically based parameterizations of large-scale condensation, shallow and deep convection, short-wave and long-wave radiation, surface fluxes of momentum, heat, moisture, and vertical diffusion. Convection is represented by a mass-flux scheme that is activated where conditional instability is present, and boundary-layer fluxes are obtained by stability-dependent bulk formulae. Land and ice temperature anomalies are determined by a simple one-layer thermodynamic model.

We conduct three sets of sensitivity experiments with the ICTP AGCM. A first ensemble of four members consists of the ICTP AGCM forced with observed SST from 1950 to 2000. In a second ensemble (ENS$_{CLIM}$) the AGCM is forced by the climatological SST derived from the CMIP3 ensembles (for each CMIP3 model we run a four member ensemble with the AGCM) and the observed SST anomalies for the 1950–2000 period. In the third ensemble (ENS$_{TOT}$), the AGCM is forced by both SST climatology and anomalies from each of the CMIP3 runs considered. The aim of these integrations is to isolate the effects of the modeled SST bias and variability on the STA teleconnection pattern.

2.3 CMIP3 model climatologies

When compared to HadISST, the JJAS-SST climatology for the CMIP3 models show generally a warm bias over the southeastern equatorial Atlantic and a cold bias in the western part (Fig. 3). This leads to a modeled eastward Atlantic equatorial zonal SST gradient during JJAS instead of the observed westward gradient. The tropical Atlantic bias is less than 2°C for MRI (Fig. 3d), while it reaches 4°C–6°C for the other four models. Focusing on the SST climatology in the Indian Ocean, all models show colder SSTs than the observations, except HADCM3 (Fig. 3c) which has a strong positive SST bias. The bias in the northern Indian Ocean, around the Indian peninsula, is distinctly stronger than 1°C and spread over most of the basin in MRI and NCAR-PCM1 (Fig. 3d,e). In the ensemble mean (Fig. 3f) the tropical Atlantic bias dominates over the Indian Ocean one. Overall, all five models depict reasonably well the main features of precipitation and low level winds climatology for the Indian and Asian monsoon system (Fig. 4a–e to be compared with Fig. 4f showing the CMAP). Noticeably, however, several models fail to properly represent the rainfall peak along the Western Ghats and the rainfall pattern around the Bay of Bengal for the Indian peninsula, and the rainfall east of Indonesia. Furthermore, the NCAR-PCM1 model shows a significant overestimation of Sahel rainfall (Fig. 4e).

3 Results

3.1 CMIP3 analysis

We begin our analysis performing a lead lag-correlation between STA and NIÑO34 for the various models and investigating the regressed response of the SSTs in the tropical band to a cold STA anomaly. Here and in the following shaded patterns in the regression maps represent the 10% statistical significance level. The regression maps are calculated using the ensemble mean for each coupled model. Given that we consider the period 1950 to 2000, 50 degrees of freedom are considered to evaluate the statistical significance.

In the GFDL model a weak and predominantly non significant correlation between the two indices is recovered (Fig. 5a) in very good agreement with the observations. The correlation coefficient (CC) for each of the GFDL ensemble members varies from −0.2 to 0.3 as in the observations. The correlation map for the ensemble mean, obtained after linearly removing the ENSO signal, displays a region of weak cooling in the eastern Pacific south of the Equator but is missing the teleconnection to the SSTs in the Indian Ocean and to the warm pool. In contrast, MPI-ECHAM5 displays
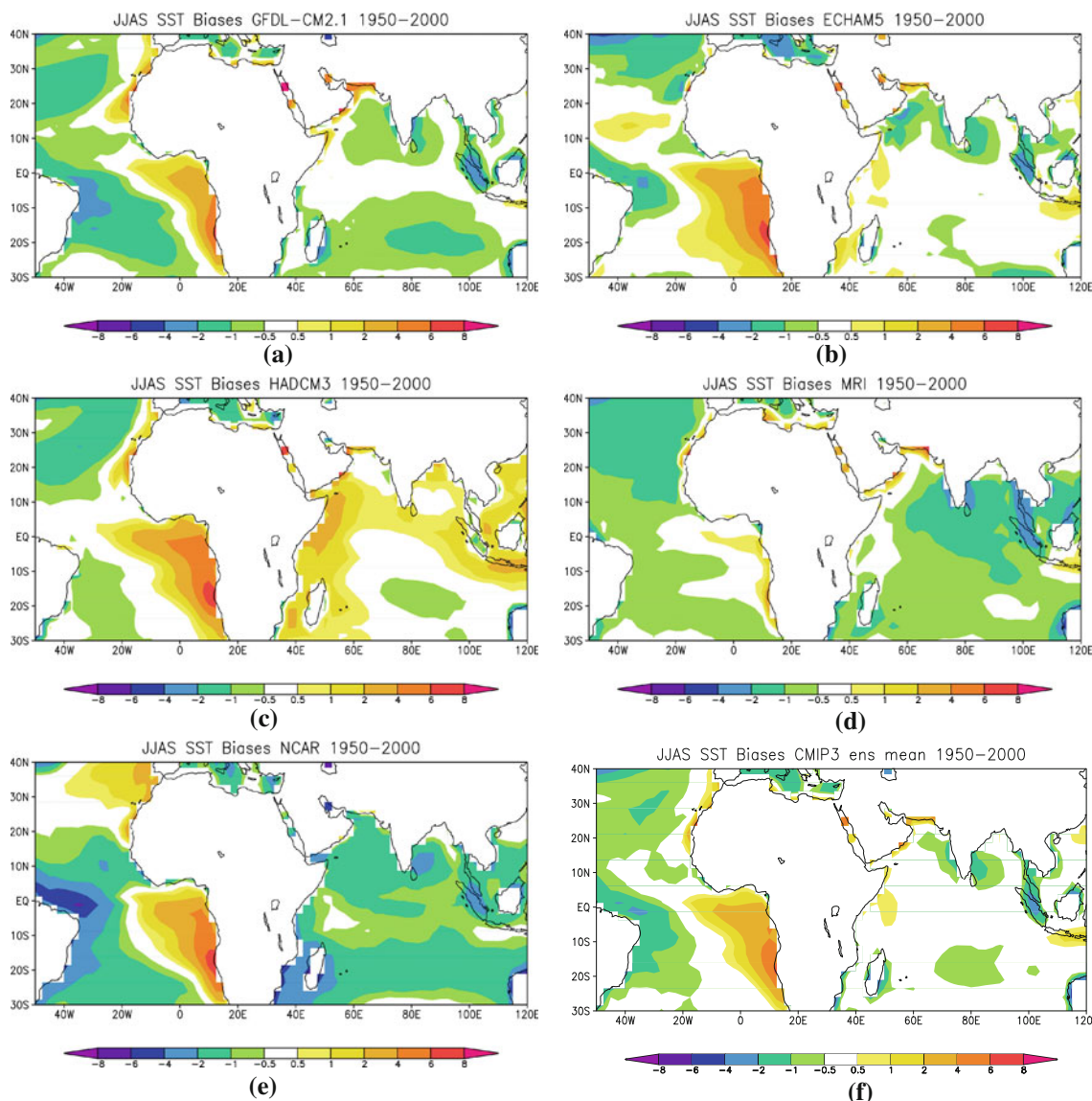
Fig. 3 SST biases in JJAS for the model ensemble averages. **a** GFDL-CM21; **b** MPI-ECHAM5; **c** HADCM3; **d** MRI; **e** NCAR-PCM1 and **f** CMIP3 ensemble mean

lead-lag correlations with opposite than observed behavior and statistically significant values (up to CC = −0.4) for NIÑO34 preceding STA anomalies by about two to four months (Fig. 5c). As a result, the SST response in this model displays a strong signal in the Pacific despite removing the linear contribution of ENSO at zero-lag (Fig. 5d). MPI-ECHAM5 has also a strong response in the Indian Ocean, concentrated in the western part of the basin, of the same sign of the observed signal but of greater amplitude. In the MRI ensemble (Fig. 5e), for three members the correlation between ENSO and STA indices are non significant at all lags and for the remaining two are weak and significant only for ENSO preceding the STA anomalies by two months at most. The SST regression map for the ensemble mean shows regions of significant cooling

in good agreement with the observations (Fig. 5f). HadCM3 has a correlation between ENSO and STA that reaches almost −0.3 at zero lag, but the ENSO effect is removed in the regression map (Fig. 5g, h). The model however does not display any correlation to the STA anomalies in the tropical Pacific and Indian Oceans. Finally, the NCAR-PCM1 ensemble shows an overall non significant or very weak lead-lag correlations (Fig. 5i) while the regression map for the ensemble mean displays significant but not realistic cooling along the western coast of South-America and in the central Pacific south of the Equator (Fig. 5j).

Although only two models display a significant correlation between STA and Indian Ocean SST anomalies, the STA-SST regression map calculated for the ensemble mean of the CMIP3 runs exhibits a cold SST anomaly in
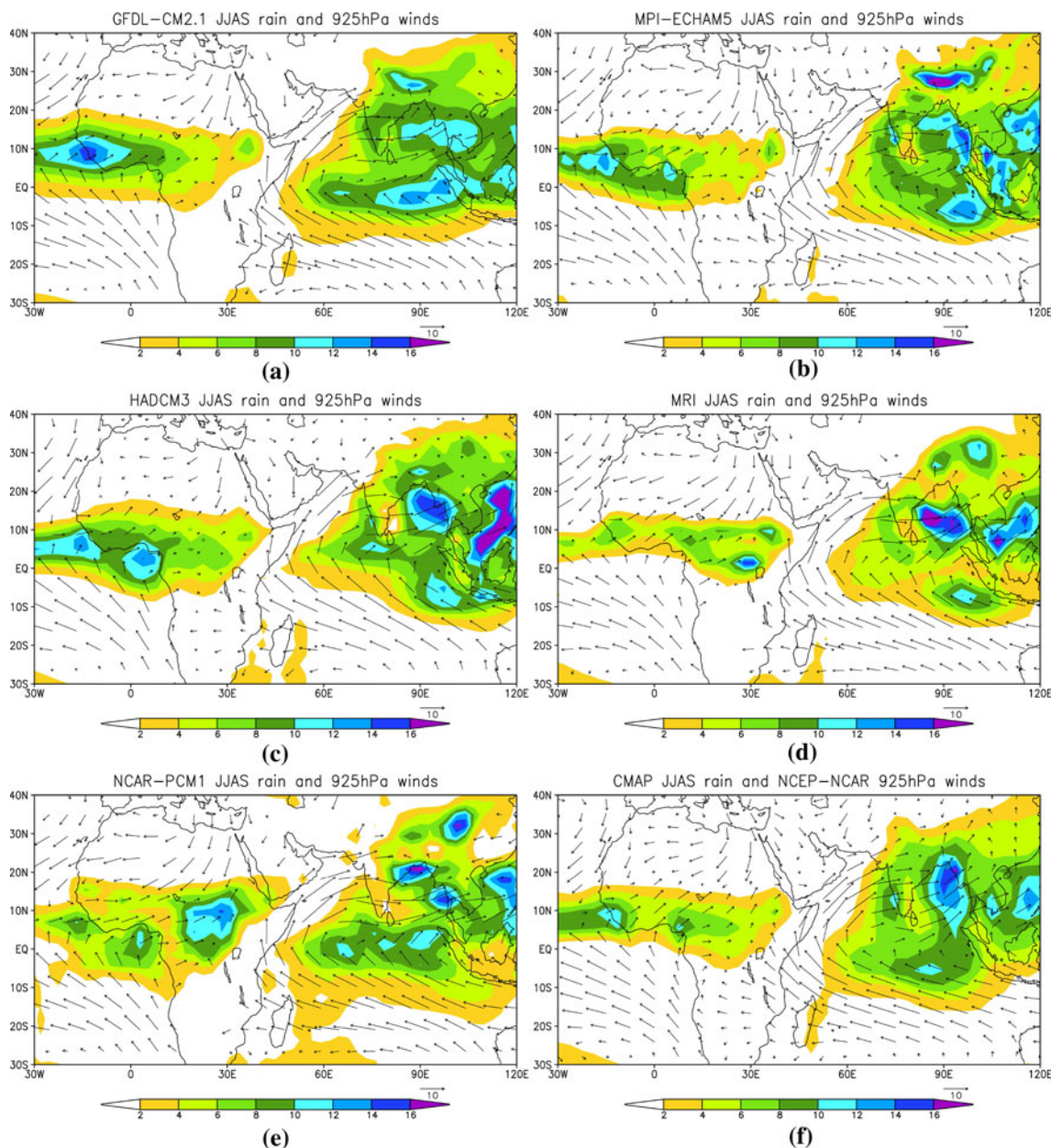
Fig. 4 Precipitation and 925 hPa wind climatology in JJAS for **a** GFDL-CM21; **b** MPI-ECHAM5; **c** HADCM3; **d** MRI; and **e** NCAR-PCM1. Panel **f** displays the observed climatology for comparison; it is derived using CMAP for precipitation and NCEP-NCAR reanalysis for near surface winds. Units are mm day^{-1} for precipitation and m s^{-1} for winds

the western Indian Ocean in response to a cold SST anomaly in the STA region in agreement with the observations (Fig. 10a). As a note of caution, it cannot be ruled out that the ENSO teleconnected signal may contribute to the regression map, given that a significant lead-lag correlations between the Nino3.4 and the STA index exists in the MPI-ECHAM5 model.

Focusing on precipitation patterns, we first analyze the response to STA SST anomalies over Africa. The GFDL model (Fig. 6a) displays a rainfall decrease on the Gulf of Guinea, extending to 20°N, and a band of positive anomaly

around 10°N. A strong rainfall increase is seen also over the Sahel. These patterns are consistent with the observations. The GFDL ensemble however overestimates the rainfall increase in the Sahelian region and extends it too far to the south into Sudan (around 5°S). Nonetheless the GFDL model reproduces well the interannual variability of the Sahel rainfall in the XX century (Biasutti et al. 2006). MPI-ECHAM5 (Fig. 6b) exhibits also a precipitation decrease in the Gulf of Guinea, accompanied by an increased rainfall further north. The anomaly over the Sahel, however, is limited to a very small region and it
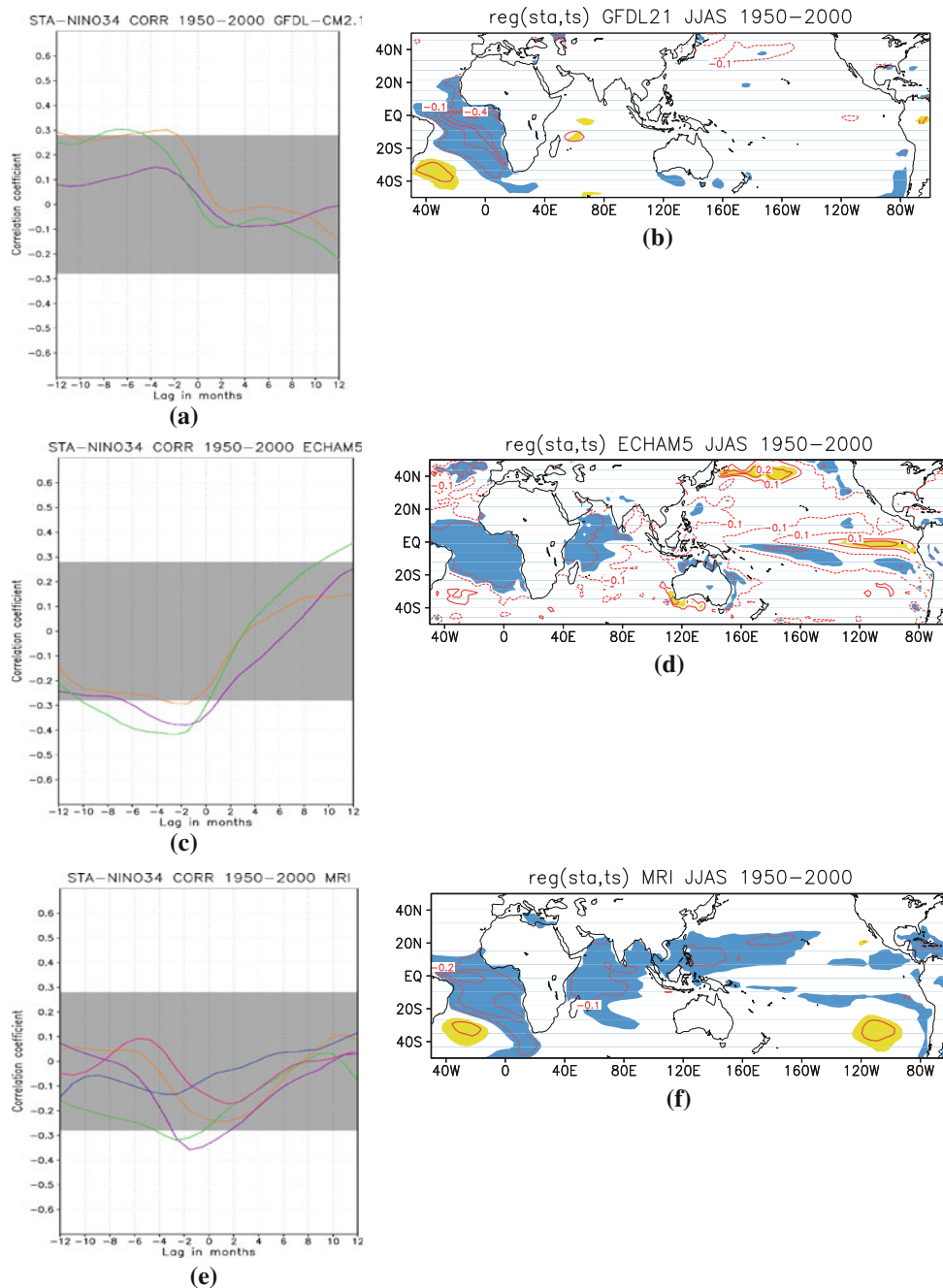
(a)

(b)

(c)

(d)

(e)

(f)

Fig. 5 Plot of the lagged correlation coefficient between the JJAS STA index and the (lagged) 4-months average NIÑO34 index as in Fig. 1a for **a** GFDL-CM2.1, **c** MPI-ECHAM5, **e** MRI, **g** HADCM3, **i** NCAR models. *White* areas indicate where the correlation is statistically significant at the 5% level; the shaded ones where the correlations is not significant. Different curves indicate different ensemble members. **b** Ensemble averages of SST regression onto the STA index for the **b** GFDL-CM2.1, **d** MPI-ECHAM5, **f** MRI, **h** HADCM3, **j** NCAR models. Units are K. All regressions are performed over the 1950–2000 period. *Shaded* areas indicate anomalies statistically significant at the 10% level in the ensemble average

reaches at most 0.1 standard deviations. Similarly for HADCM3 (Fig. 6d), the response to the STA cooling in the Sahelian region is weak compared to the CRU data, and it is accompanied by a strong negative precipitation anomaly extending between 5°N and 15°S in the Gulf of Guinea. In

contrast, MRI (Fig. 6c) does not reproduce the rainfall decrease over the Gulf of Guinea, and the dry anomaly is seen further west, over the ocean, while the Sahel shows a weak rainfall decrease. Finally, the NCAR-PCM1 model (Fig. 6e) displays a different response to cold SST
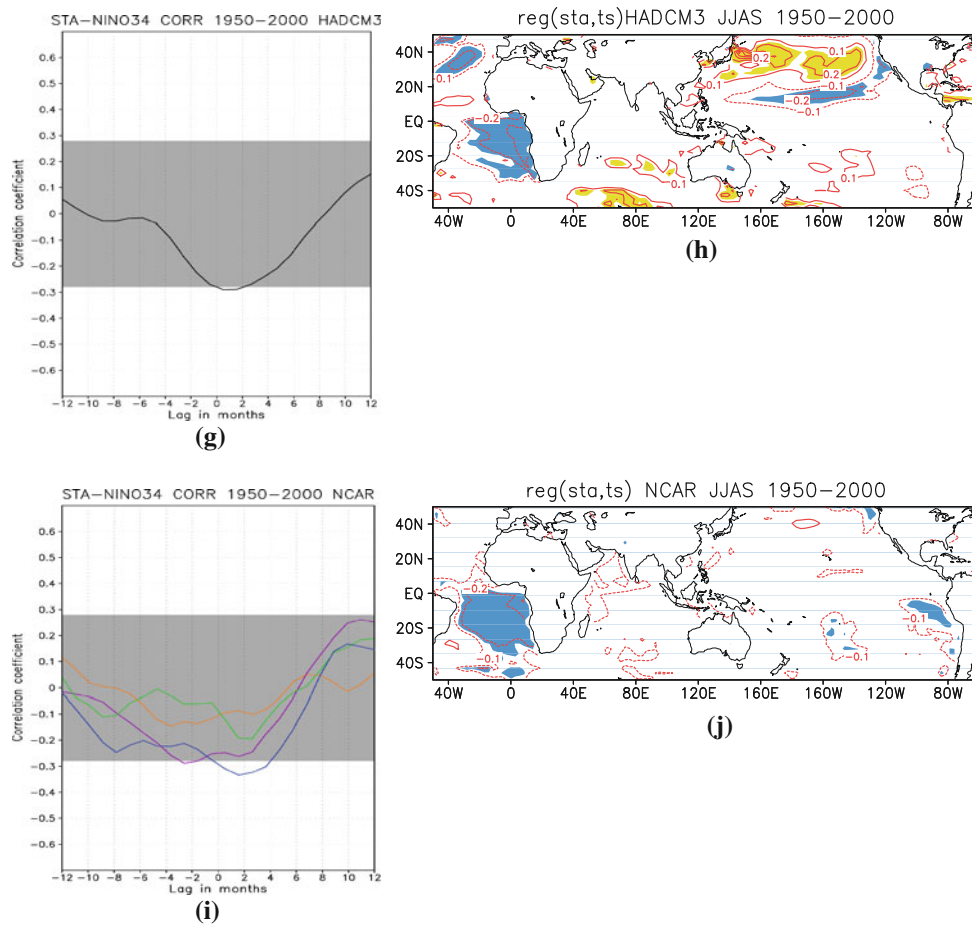
Fig. 5 continued

anomalies in the STA region compared to the observations and the other models. The precipitation patterns along the coast of West-Africa are shifted toward the south: a positive anomaly extends to the Gulf of Guinea and a negative anomaly is seen below the equator. A significant decrease of precipitation is also evident over the Sahel, contrary to the observed signal. Except for the MRI and NCAR-PCM1 models, the precipitation patterns over Africa are consistent with a Gill-Matsuno response to heat anomalies in the tropical Atlantic that lead to low-level divergence and decreased rainfall near the Guinea Coast, as pointed out by, e.g., Vizy and Cook (2001) and Giannini et al. (2003).

Moving to the Indian region, the patterns from GFDL, MPI-ECHAM5, HADCM3 agree with the observed strengthening of the Indian monsoon in response to a cold STA SST anomaly. In GFDL and ECHAM5 the rainfall increase displays a similar structure, while it extends westward over the Arabian Sea in HADCM3. In ECHAM5 a decrease in precipitation further to the east over Indonesia is also evident. The rainfall response in this three models is consistent with the findings in Kucharski et al. (2007,

2008, 2009), where an idealized AGCM, eventually coupled to an ocean model only in the Indian basin, was used. For MRI the precipitation response over India and its surrounding is weaker compared to the above models and the observations. The rainfall increase is limited to a small region in the eastern Indian peninsula and the equatorial rainfall decrease extends to the southern part of India. The NCAR-PCM1 does not reproduce the precipitation response over India at all, even though it shows a rainfall pattern similar to MPI-ECHAM5 and HADCM3 in the equatorial Indian Ocean.

In the ensemble mean the rainfall regression resembles the observed one over India and Africa but the intensity of the signal is weaker than observed except for the southeastern Indian Ocean, where it is too strong (Fig. 10b). The CMIP3 ensemble mean confirms the existence of a symmetric structure north and south of the equator in the Indian ocean in response to the STA SST anomaly as pointed out by Kucharski et al. (2009). A precipitation increase is seen at about 10°N–30°N and 20°S–5°S, whereas a decrease is seen in the equatorial Indian Ocean.
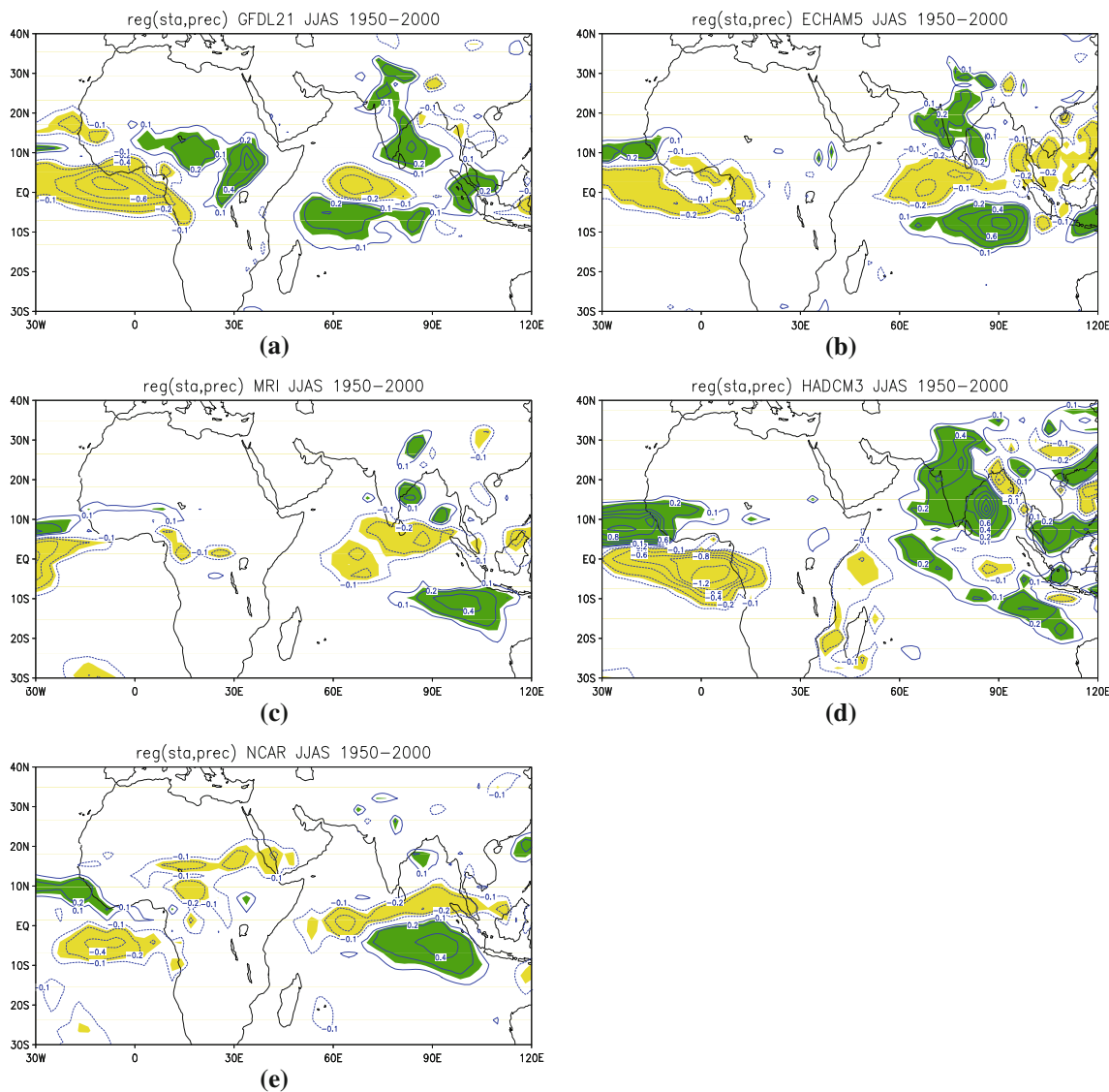
Fig. 6 Ensemble average of precipitation regression onto the STA index over 1950–2000 for the **a** GFDL-CM21, **b** MPI-ECHAM5, **c** MRI, **d** HADCM3, and **e** NCAR-PCM1 models. Shaded areas represent anomalies that are statistically significant at the 10% level; *Green/dark grey* and *yellow* (*light grey*) indicate positive and negative anomalies, respectively. Units are mm/day

As already mentioned, the physical mechanism by which cold SST anomalies in the STA region cause rainfall anomalies over Africa and India is a simple Gill-Matsuno-type response: A cooling over the south tropical Atlantic triggers a southwestward pressure gradient, together with northeastward surface winds, over Africa and the Indian basin. Therefore a low level divergence combined with a decreased rainfall is found over the western equatorial Africa and low level convergence with increased rainfall occupies the eastern part side of the continent and the Indian basin.

To conclude our investigation, we perform a regression analysis to investigate the surface pressure (SP) and low and upper level wind responses in the coupled GCMs.

Figure 7a,b,c,d,e displays the SP response for the CMIP3 models under consideration. In all five coupled GCMs the response to a cold STA anomaly consists of a high pressure over the South Tropical Atlantic and a lower pressure in the Indian Ocean. This leads to an overall pressure gradient from the Indian Ocean towards the South Tropical Atlantic. However, whereas the SP response in the STA region is similarly positioned in all models, the location of the pressure minimum in the Indian basin varies largely. Most models display a pressure minimum in the south-eastern Indian Ocean, which is not observed, and may be related to the SST bias in the Atlantic basin which shifts the overall response to the southern hemisphere (see also Sect. 3.2). Near the equator the low-level wind
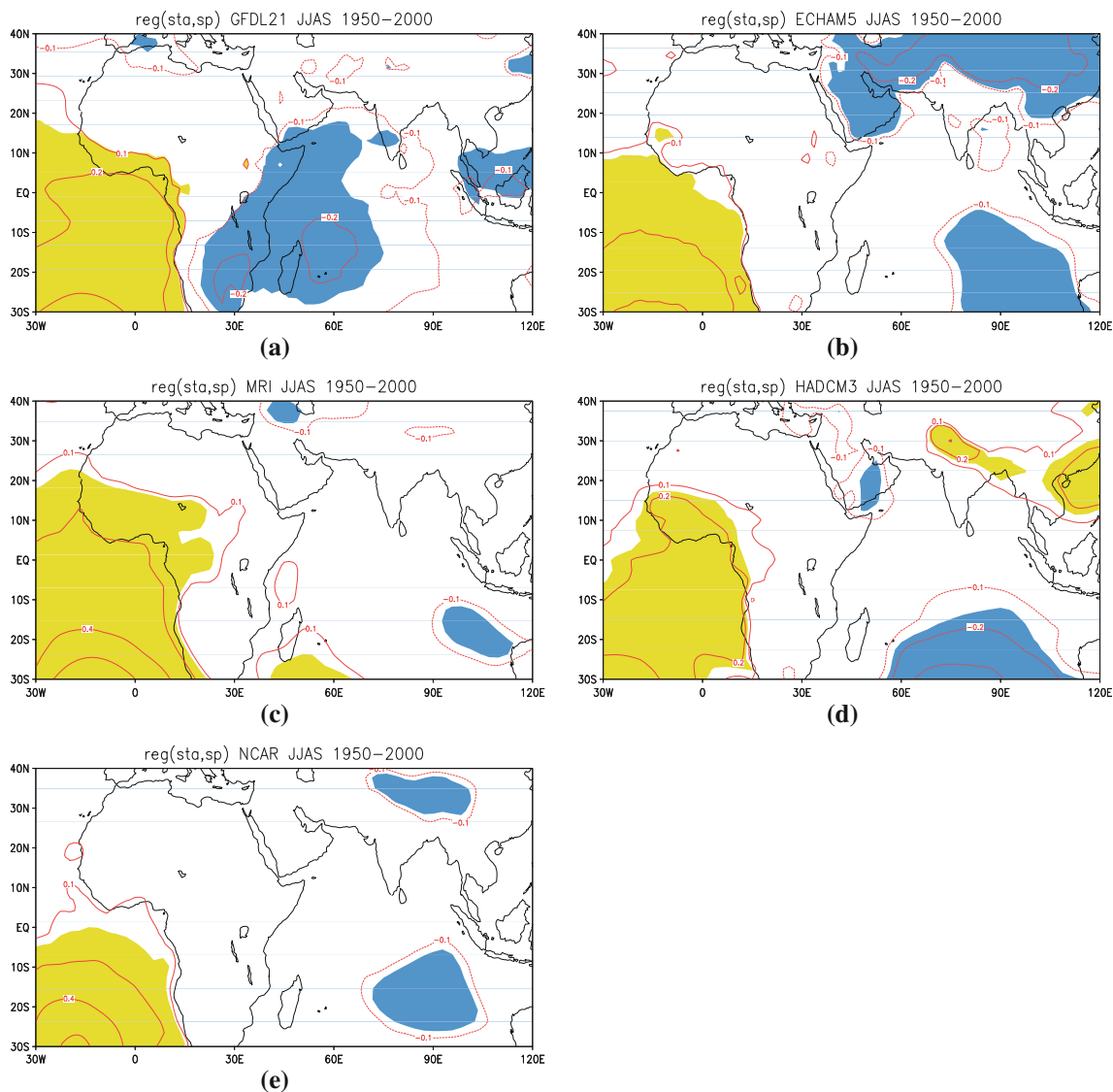
Fig. 7 Ensemble regression of surface pressure onto STA for the **a** GFDL-CM21, **b** MPI-ECHAM5, **c** MRI, **d** HADCM3, and **e** NCAR-PCM1 models. *Shaded* areas present the statistical significant anomalies at the 10% level. *Blue* (*dark grey*) and *yellow* (*light grey*) indicate respectively the negative and positive anomalies. Units are hPa

responses in the CMIP3 outputs (Fig. 8a,b,c,d,e) provide a useful illustration of the STA-induced circulation. In all models westerly wind anomalies develop in response to a cold STA in the western African region as in the observations, but their exact position vary. Consequently not all models reproduce the observed divergence along the Guinea Coast, and in turn the associated rainfall reduction. This deficiency is most likely due to the warm bias in the tropical Atlantic. Focusing on the Indian basin, all models but GFDL replicate the observed strengthening of the Somali Jet and the convergent flow over India. The GFDL output, on the other hand, displays an anticyclonic flow in the Arabian Sea region. Both MRI and NCAR-PCM1 show the intensification of the Somali Jet and the low-level

convergence, but only a weak rainfall response. This is related to the strong cold bias in the northern Indian Ocean in both models (Fig. 3d,e), which reduces the moisture availability even in the presence of low-level convergence. Further to the east, all models responses are characterized by equatorial westerlies and a cyclonic flow in the south eastern Indian Ocean (around 20°S) that are not observed. The observed low-level cyclone in the southern hemisphere is indeed located in the western Indian Ocean. This eastward shift and strengthening of the southern hemispheric response in the CMIP3 CGCMs with respect to observations is likely related to the warm bias in the STA region.

In the CMIP3 ensemble mean response (Fig. 10c, d), a negative SP anomaly and a corresponding low level wind
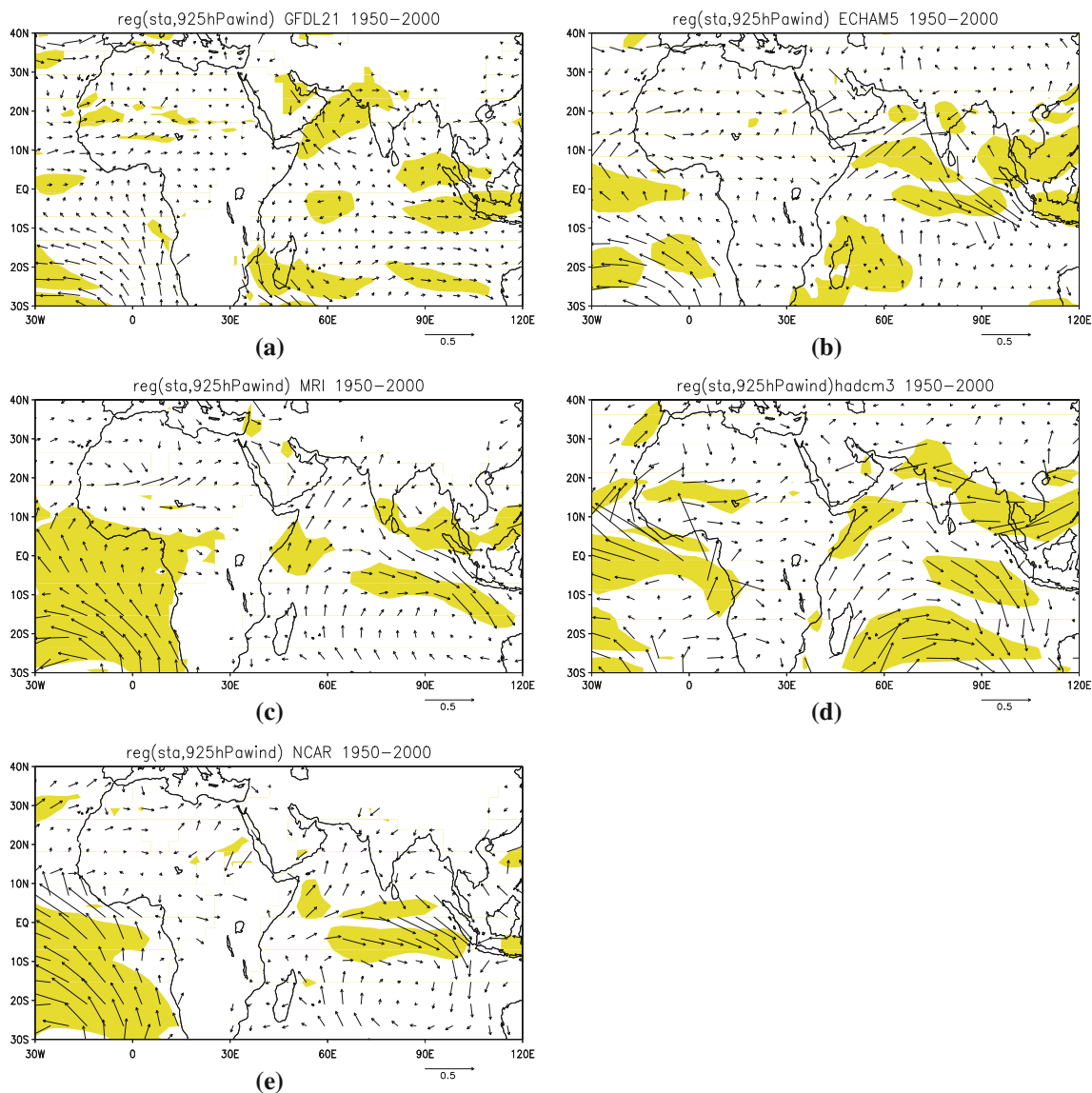
Fig. 8 Ensemble regression maps of near surface wind onto the STA index for the **a** GFDL-CM21, **b** MPI-ECHAM5, **c** MRI, **d** HADCM3, and **e** NCAR-PCM1 models. *Shaded* areas present the statistical significant anomalies at the 10% level. Units are m/s

cyclone are found over the south-east Indian Ocean. The SP anomaly in the northern part of the Indian basin is weaker than in the NCEP reanalysis. On the other hand, the southwesterly wind anomaly along the eastern coast of Africa and the cyclonic pattern over the central Bay of Bengal, both represented in the ensemble mean, are in better agreement with the observed signal.

Figure 9 shows the 200 hPa wind regressed signal to cold SST anomalies in the STA region. Four out of five GCMs display an equatorial easterly upper level wind response as in the observations. One noticeable exception is the GFDL model (Fig. 9a) that produces equatorial wind anomalies of opposite direction. The pair of anticyclones found in the observations (Fig. 2j) in the southern and northern subtropics at about 50°E, 25°S and 50°E, 30°N is evident only in the

HADCM3 model. The remaining CGCMs reproduce only the southern anticyclone, while the northern is missing. This is confirmed by the upper level wind response in the CMIP3 ensemble mean (Fig. 10e) where an anticyclone is evident only around 50°E, 25°S. Nevertheless, in the northern Indian Ocean the zonal wind shear for the CMIP3 ensemble mean is clearly anticyclonic—despite the absence of the upper-level anticyclone—as for individual models, with the exception of the GFDL one. When compared to the low-level, the amplitude of the upper-level wind response is in better agreement with the observed signal, apart from the GFDL model in which the intensity of the anomalies—of opposite sign than observed—is much reduced.

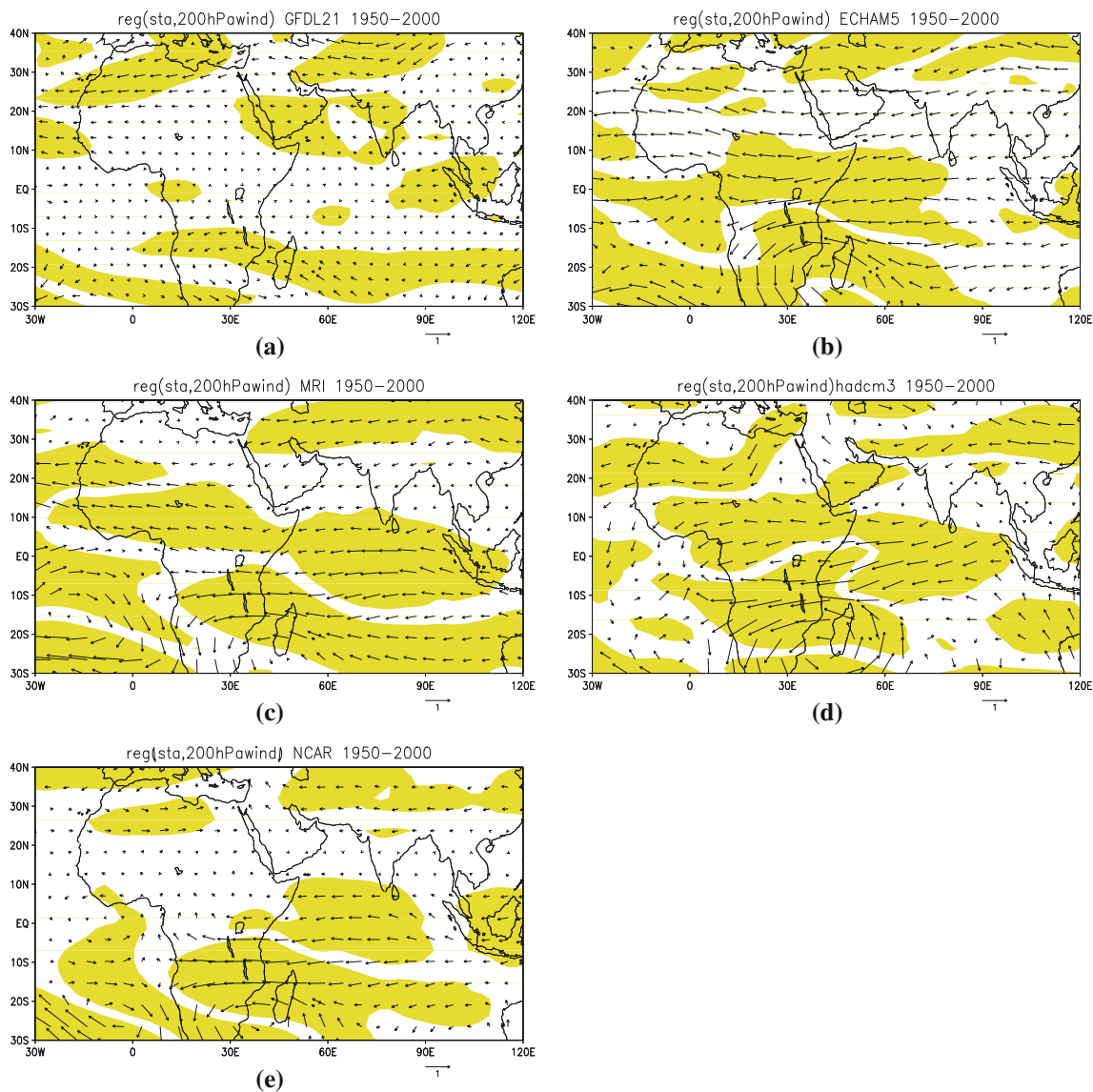In summary, the suite of CMIP3 CGCMs analyzed in this work reproduces to some extent the STA-Indian

Fig. 9 Ensemble regression maps of the 200 hPa wind field onto the STA index for the **a** GFDL-CM21, **b** MPI-ECHAM5, **c** MRI, **d** HADCM3, and **e** NCAR-PCM1 models. *Shaded* areas indicate the statistical significant anomalies at the 10% level. Units are m/s

Monsoon teleconnection. However, only some of the "ingredients" of the Gill-Matsuno mechanism in response to STA SST anomalies are well reproduced. The precipitation signal over India and Africa in the CMIP3 ensemble mean is in good agreement with the observations. The rainfall response to a cold STA anomaly over India is consistent with a pressure minimum over southern Saudi Arabia that leads to an intensification of the Somali jet and thus low-level convergence over India (Fig. 10d). However, the upper- and low-level wind patterns in the eastern Indian Ocean barely resemble observations. In addition, the modeled STA response over the Indian Ocean is much stronger south than north of the equator, but almost symmetric in the observations; the teleconnection in the GCMs is weaker than observed; and the low level wind direction in the south-east Indian Ocean basin is opposite to the observations.

It is likely that the strong SST bias in the tropical Atlantic, common to most of the coupled models, plays an important role in the weak teleconnection signal. Also, the SST variability related to the STA index in the CMIP3 models may differ significantly from the observed. We further investigate the impacts of the SST bias and variability in the tropical Atlantic on the STA teleconnection by performing idealized experiments using the ICTP AGCM described in Sect. 2.
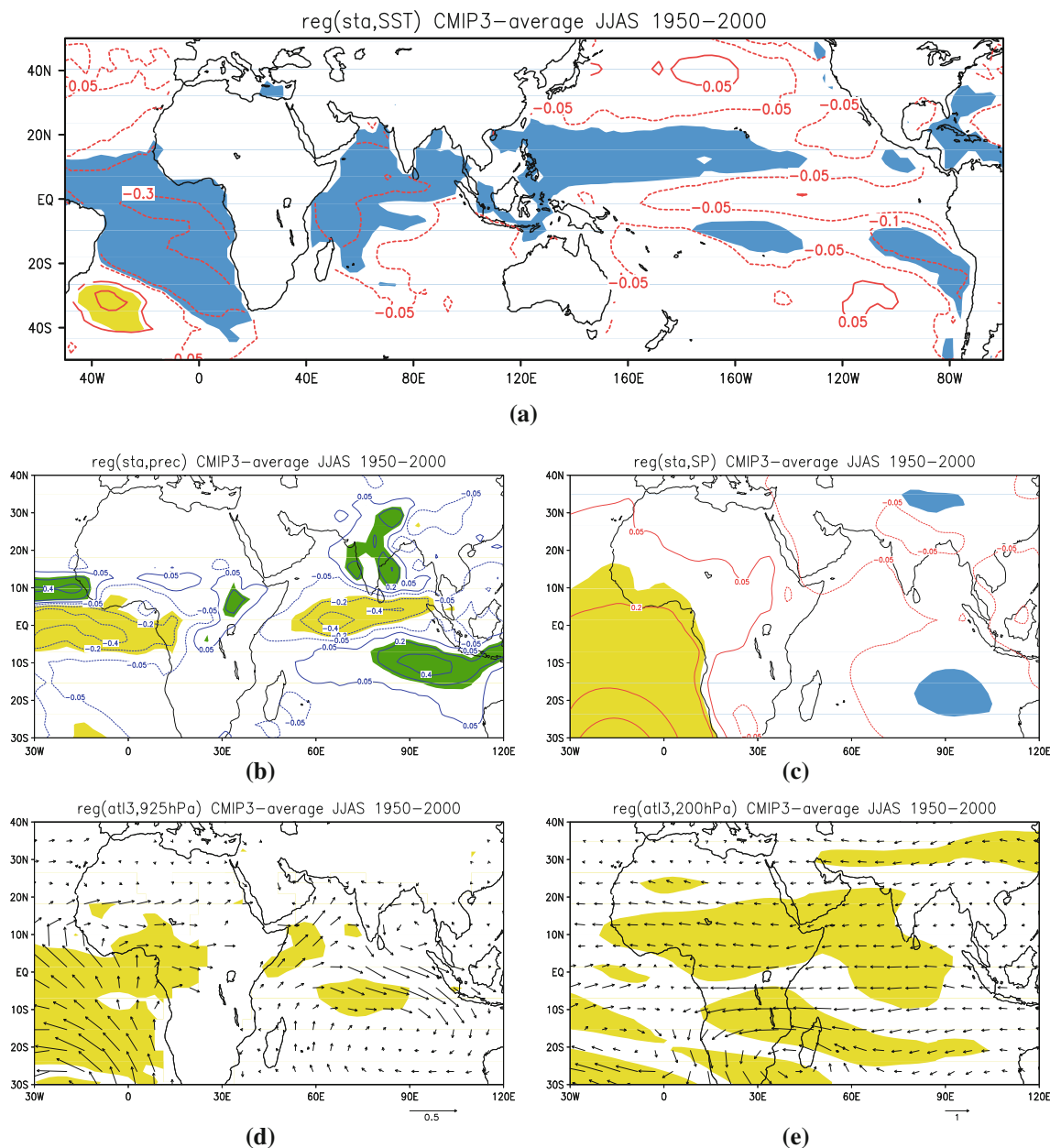
Fig. 10 CMIP3 multi-model ensemble mean regression of **a** SST; **b** Precipitation; **c** Surface pressure; **d** 925 hPa wind; and **e** 200 hPa wind onto the STA index. *Shaded areas* represent the anomalies that are statistically significant at the 10% level. Units are K, mm day^{-1}, hPa, m s^{-1} for SST, precipitation, surface pressure and wind respectively

3.2 Sensitivity experiments

We conduct three sets of experiments with the ICTP AGCM:

– *CNTRL*: A control ensemble of four runs where the ICTP AGCM is forced with observed SST from 1950 to 2000;
– ENS$_{CLIM}$: A set of sensitivity ensembles, each of four members, in which the AGCM is forced by the superimposition of climatological SST derived from the ensemble mean of each of the CMIP3 models and by the observed SST anomalies over the 1950–2000 period;
– ENS$_{TOT}$: A series of runs equal to the total number of CMIP3 outputs considered in which the AGCM is forced by the full SST field generated by the coupled models.

The aim of these sensitivity experiments is to isolate the effects of the modeled SST bias and interannual variability on the STA teleconnection pattern.

Here again we present a simple correlation-regression analysis comparing the STA response in the ensemble means of each set of runs. Figures 11, 12 and 13 show the STA response in (a) precipitation, (b) surface pressure, (c) 200 hPa wind for *CNTRL*, ENS$_{CLIM}$ and ENS$_{TOT}$, respectively. In the *CNTRL* run, the precipitation signal consists of a decrease over the Coast of Guinea, and an increase in the Sahel and Indian region. The modeled pattern of rainfall increase over the Indian basin is symmetric with respect to the equator as in the observations, and the SP map shows a positive anomaly over the western coast of Africa and a maximum negative anomaly over the Indian region. In addition, a pair of anticyclones is clearly visible in the upper-level wind response. These regression maps are in good agreement with the observations and all together suggest that the ICTP AGCM is capable of simulating the Gill-Matsuno teleconnection.

By forcing the model with the CMIP3 climatologies, the ICTP AGCM reproduces a response to the STA anomalies closer to the observed one than the CMIP3 ensemble mean (Fig. 12). However, compared to the *CNTRL* run, in ENS$_{CLIM}$ the rainfall response in the Atlantic/west African region is substantially shifted to the south. This leads to a change in sign of the rainfall anomalies at the Guinea coast. The southward shift is also noticeable in the Indian region, although it is weaker than over western Africa. The rainfall

signal in the northern Indian region has the opposite sign compared to the control simulation. The SP response in ENS$_{CLIM}$ is weaker than in *CNTRL*, and a significant negative anomaly occupies eastern India. Finally, the upper-level wind pattern is characterized by easterly winds, but there is no sign of the observed anticyclonic patterns around 50°E, 25°S and 50°E, 30°N. The differences between individual simulations in the ENS$_{CLIM}$ ensemble are relatively small, suggesting that the reduced Tropical Atlantic climatological SST gradient—common to all CMIP3 climatologies—causes the response to weaken, while the SST bias over the Indian Ocean plays a minor role. When the AGCM is forced with both SST climatology and anomalies from the CMIP3 data, the response is even weaker in all fields (Fig. 13), and the 200 hPa wind map shown in Fig. 13d resembles that of the CMIP3 ensemble mean (Fig. 10e). Furthermore, individual integrations within the ENS$_{TOT}$ ensemble display larger intra-ensemble differences over the Indian basin (not shown), with the GFDL SST-based run being the closest to the corresponding integration from ENS$_{CLIM}$. This is consistent with the GFDL model having the most realistic and strongest STA variability, as suggested by the regression pattern over the south tropical Atlantic shown in Fig. 5b.

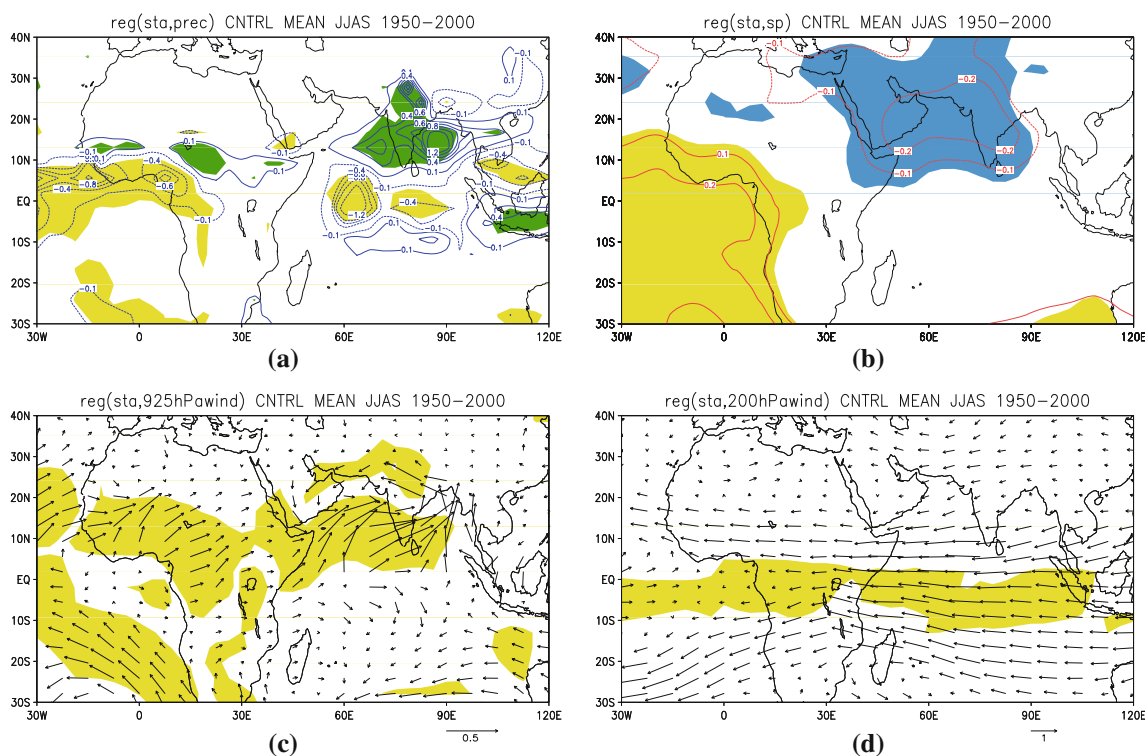Despite several important differences between the ICTP AGCM and CMIP3 responses to the STA SST anomalies,

Fig. 11 Regression maps of **a** Precipitation; **b** Surface pressure; **c** 925 hPa wind; **d** 200 hPa wind regression onto the STA index for the CNTRL ensemble. *Shaded* areas represent the anomalies that are statistically significant at the 10% level. Units are K, mm day^{-1}, hPa, m s^{-1} for SST, precipitation, surface pressure and wind, respectively
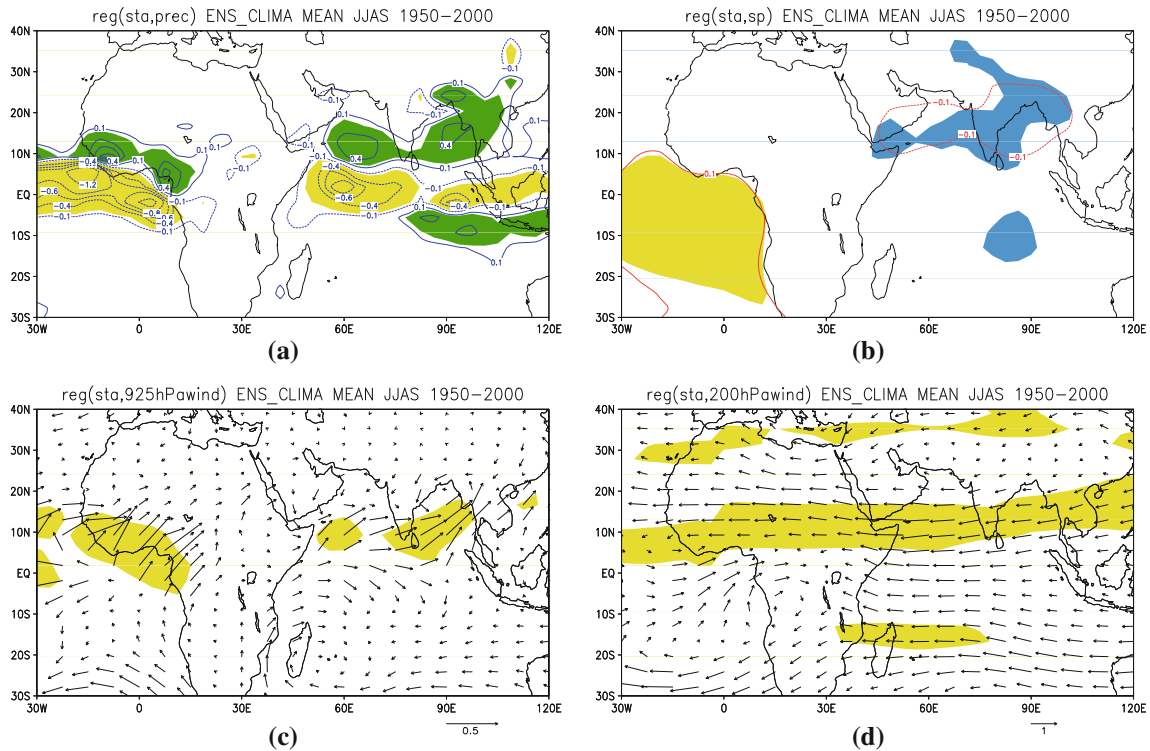
Fig. 12 Regression maps of **a** Precipitation; **b** Surface pressure; **c** 925 hPa wind; **d** 200 hPa wind regression onto the STA index for the ENS_CLIMA ensemble. Shaded areas represent the anomalies that are statistically significant at the 10% level. Units are K, mmday^{-1}, hPa, m s^{-1} for SST, precipitation, surface pressure and wind, respectively
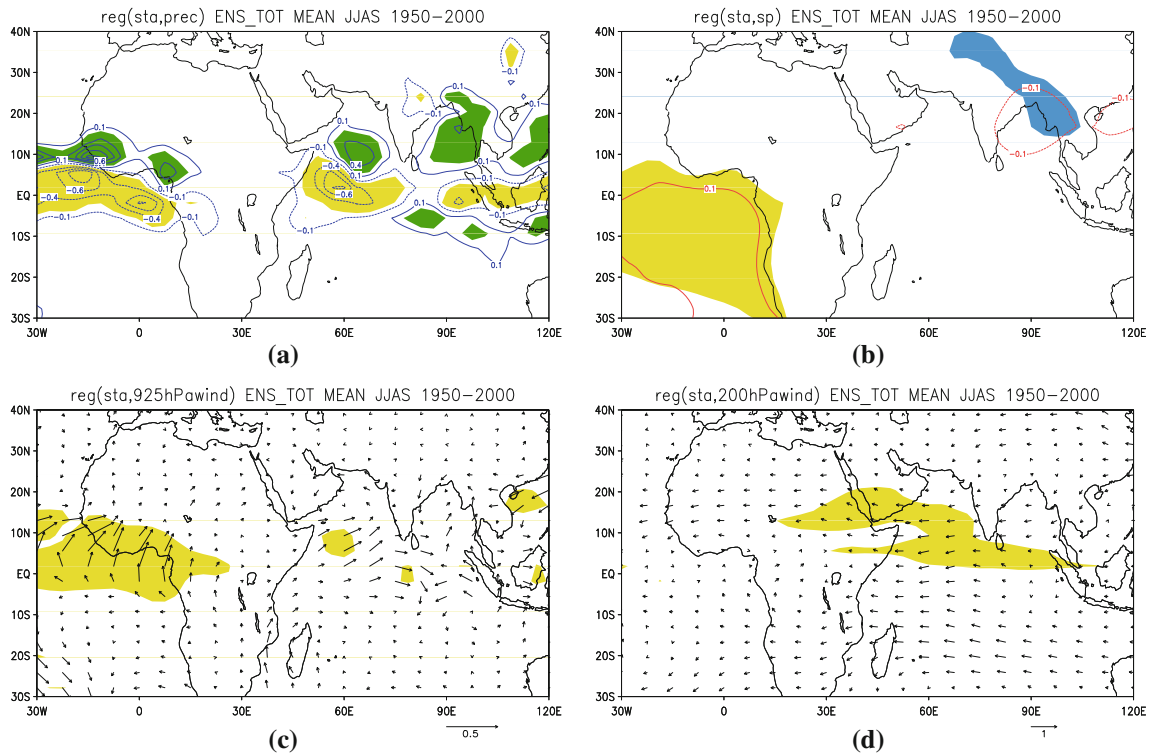

Fig. 13 Regression maps of **a** Precipitation; **b** Surface pressure; **c** 925 hPa wind; **d** 200 hPa wind regression onto the STA index for the ENS_TOT ensemble. *Shaded* areas represent the anomalies that are statistically significant at the 10% level. Units are K, mm day^{-1}, hPa, m s^{-1} for SST, precipitation, surface pressure and wind, respectively

it is shown that the teleconnection weakens in the northern hemisphere, and the signal is shifted south of the equator compared to the control run. Therefore, the SST biases and reduced variabilities in the STA region are partially responsible for the inability of the coupled models to properly reproduce the Gill-Matsuno teleconnection in the northern Indian Ocean.

We also tested the role of the large coupled model errors in land temperatures in causing the differences between the AGCM runs forced by CMIP3 SSTs and the coupled model outputs. We performed a fourth ensemble forcing the ICTP-AGCM with both the land temperatures and the SST climatologies from the CMIP3 models. We did not notice any significant change in the representation of the teleconnection into the Indian Ocean, indicating that land biases are not key.

Summarizing, the ICTP AGCM forced by the CMIP3 SST climatologies can reproduce only in part the weakening of the Gill-Matsuno teleconnection signal found in the CMIP3 ensemble. Also, the ensemble spread from individual AGCM runs forced with different CMIP3 model climatologies is far more limited compared to that from the CMIP3 models. This spread increases if the CMIP3 SST anomalies are used to force the AGCM, but the responses in the ICTP AGCM integrations still do not resemble the CMIP3 outputs. This suggests that intra-model differences (e.g. parameterization of surface fluxes, boundary layer scheme, convection and radiation schemes) play an important role in the representation of the Gill-Matsuno STA-Indian Ocean teleconnection.

4 Discussion and summary

In this work we document how state-of-the-art coupled models, and in particular five models within the CMIP3 ensemble, represent the teleconnection between the south tropical Atlantic and the Indian Ocean basin. We found that four out of five models and the ensemble mean display a teleconnection between the Tropical Atlantic and the Indian Ocean region that is consistent with observations: A cold (warm) STA SST anomaly intensifies (weakens) the Somali jet, and leads to an upper-level easterly (westerly) equatorial anomalous wind with the tendency for anticyclonic (cyclonic) shear in the subtropical regions. The rainfall over India and in the southern Indian Ocean increases (decreases), whereas rainfall anomalies of opposite sign are observed in the equatorial Indian Ocean. Additionally, over the Indian Ocean a small, but statistically significant cooling of the SST in the western side of the basin is also found.

However, the amplitude of the CMIP3 response to a STA anomaly in various fields, from rainfall to upper and lower winds, is small compared to the observations and to the response found in AGCM-only simulations forced by observed SSTs. The presence of large biases in the tropical Atlantic region in both the SST climatology and interannual variability of the CMIP3 simulations is responsible for the reduced amplitude. Indeed, when the ICTP AGCM— that reproduces correctly the Gill-Matsuno response if forced by observed SSTs—is forced with SST climatologies from the CMIP3 ensemble superimposed to the observed anomalies, the rainfall response is reversed in sign in the Gulf of Guinea and in the northern Indian region, overall reduced over Asia, and shifted to the south of the equator. The surface pressure and upper-level wind responses weaken as well, particularly in the northern hemisphere. If the ICTP AGCM is forced with the full SST field (climatologies and anomalies) from the CMIP3 models, then the STA teleconnection to the Indian basin is further reduced in strength and the simulated response is partially consistent with the CMIP3 ensemble output. The warm bias in the South Tropical Atlantic is responsible for the southward shift of the teleconnected response: The heat source of the STA anomalies is shifted to the south in the CMIP3 model ensemble, favoring the southern hemispheric component of the response, while weakening the northern hemispheric one. The large mean SST bias in the STA region in the CMIP3 runs is also likely the cause of the weaker than observed interannual variability in the tropical Atlantic.

When comparing the CMIP3 integrations with the sensitivity runs, however, we find many intra-model differences that are not accounted for and are related to the different physical parameterizations used in the coupled GCMs.

We believe it is important to document how the state-of-the-art CMIP3 models reproduce this simple Gill-Matsuno teleconnection mechanism within the broader goal of understanding and predicting climate variability. A better representation of teleconnections in the tropics in coupled models will increase our confidence in the climate change projections provided by the same models. The climate modeling community would profit from reducing the SST bias in the tropical Atlantic, not only for the representation of rainfall responses over Africa, but also in the Indian basin.

References

Adler RF, Huffman GL, Chang A et al (2003) The version-2 global precipitation climatology project (GPCP) monthly precipitation analysis (1979-present). J Hydrometeor 4(6):1147–1167

Allan RJ, Ansell TJ (2006) A new globally-complete monthly historical gridded mean sea level pressure data set (HadSLP2). J Clim 19:5816–5842

Annamalai H, Hamilton K, Sperber KR (2007) The South Asian summer monsoon and its relationship with ENSO in the IPCC AR4 simulations. J Clim 20:1071–1092

Biasutti M, Sobel A, Kushnir Y (2006) AGCM precipitation biases in the tropical Atlantic. J Clim 19:935–958

Bourke W (1974) A multilevel spectral model. I. Formulation and hemispheric integrations. Mon Weather Rev 102:687–701

Chang P, Fang Y, Saravanan R, Ji L, Seidel H (2006) The cause of the fragile relationship between the Pacific El Niño and the Atlantic Niño. Nature 443:324–328

Chen T-C (2003) Maintenance of summer monsoon circulations: a planetary perspective. J Clim 16:2022–2037

Delworth TL, Broccoli AJ, Rosati A, Stouffer RJ, Balaji V, Beesley JA, Cooke WF, Dixon KW, Dunne J, Dunne KA, Durachta JW, Findell KL, Ginoux P, Gnanadesikan A, Gordon CT, Griffies SM, Gudgel R, Harrison MJ, Held IM, Hemler RS, Horowitz LW, Klein SA, Knutson TR, Kushner PJ, Langenhorst AR, Lee H, Lin S, Lu J, Malyshev SL, Milly PCD, Ramaswamy V, Russell J, Schwarzkopf MD, Shevliakova E, Sirutis JJ, Spelman MJ, Stern WF, Winton M, Wittenberg AT, Wyman B, Zeng F, Zhangc R (2006) GFDL's CM2 global coupled climate models—Part 1: formulation and simulation characteristics. J Clim 5:643–674

Enfield D, Mayer D (1997) Tropical Atlantic sea surface temperature variability and its relation to El Niño-Southern oscillation. J Geophys Res 102:929–945. doi:10.1029/96JC03296

Enfield DB, Mestas-Nunez AM, Mayer DA, Cid-Serrano L (1999) How ubiquitous is the dipole relationship in tropical Atlantic sea surface temperatures?. J Geophys Res 104:7841–7848

Giannini A, Saravanan R, Chang P (2003) Oceanic forcing of Sahel rainfall on interannual to interdecadal time scales. Science 302:1027–1030

Gill AE (1980) Some simple solutions for heat-induced tropical circulations. Q J Roy Meteor Soc 106:447–462

Gordon C, Cooper C, Senior C, Banks H, Gregory J, Johns T, Mitchell J, Wood R (2000) The simulation of SST, sea ice extents and ocean heat transports in a version of the Hadley Centre coupled model without flux adjustments. Clim Dyn 16:147–168

Handoh I, Bigg GR, Matthews A, Stevens D (2006) Interannual variability of the Tropical Atlantic independent of ENSO: Part II. The South Tropical Atlantic. Int J Climatol 26:1957–1976. doi:10.1002/joc.1342

Held IM, Suarez MJ (1994) A proposal for the intercomparison of the dynamical cores of atmospheric general circulation models. Bull Am Meteor Soc 75:1825–1830

Hu ZZ, Huang B (2007) Physical processes associated with the tropical Atlantic SST gradient during the anomalous evolution in the southeastern ocean. J Clim 20:3366–3378

Huang B, Schopf P, Shukla J (2004) Intrinsic ocean-atmosphere variability in the tropical Atlantic Ocean. J Clim 17:2058–2077

Janicot S, Harzallah A, Fontaine B, Moron V (1998) West African monsoon dynamics and eastern equatorial Atlantic and Pacific SST Anomalies. J Clim 11:1874–1882

Joly M, Voldoire A (2009) The global monsoon variability simulated by CMIP3 coupled climate models. J Clim 22:3193–3209

Joly M, Voldoire A (2010) Role of the Gulf of Guinea in the inter-annual variability of the West African monsoon: what do we learn from CMIP3 coupled simulations?. Int J Climatol 30:1843–1856. doi:10.1002/joc.2026

Jungclaus JH, Keenlyside N, Botzet M, Haak H, Luo JJ, Latif M, Marotzke J, Mikolajewicz U, Roeckner E (2006) Ocean circulation and tropical variability in the coupled model ECHAM5/MPI-OM. J Clim 19:3952–3972

Kalnay E, Kanamitsu M, Kistler R, Collins W, Deaven D, Gandin L, Iredell M, Saha S, White G, Woollen J, Zhu Y, Chelliah M, Ebisuzaki W, Higgins W, Janowiak J, Mo C, Ropelewski C, Wang J, Leetmaa A, Reynolds R, Jenne R, Joseph D (1996) The NCEP/NCAR 40-year reanalysis project. Bull Am Meteorol Soc 77:431–437

Kim H-J, Wang B, Ding Q (2008) The global monsoon variability simulated by CMIP3 coupled climate models. J Clim 21:5271–5293

Kucharski F, Molteni F, Bracco A (2006) Decadal interactions between the western tropical Pacific and the North Atlantic oscillation. Clim Dyn 26:79–91. doi:10.1007/s00382-005-0085-5

Kucharski F, Bracco A, Yoo J, Molteni F (2007) Low-frequency variability of the Indian Monsoon-ENSO relationship and the Tropical Atlantic: the weakening of the 1980s and 1990s. J Clim 20:4255–4266

Kucharski F, Bracco A, Yoo J, Molteni F (2008) Atlantic forced component of the Indian monsoon interannual variability. Geophys Res Lett 33:L04706. doi:10.1029/2007GL033037

Kucharski F, Bracco A, Yoo J, Tompkins A, Feudale L, Ruti P, Dell'Aquila A (2009) A simple Gill-Matsuno-type mechanism explains the Tropical Atlantic influence on African and Indian Monsoon rainfall. Q J Roy Meteor Soc 135:569–579. doi:10.1002/qj.406

Kucharski F, Bracco A, Barimalala R, Yoo JH (2010) Contribution of the eastwest thermal heating contrast to the South Asian Monsoon and consequences for its variability. Clim Dyn. doi:10.1007/s00382-010-0858-3

Latif M, Grötzner A (2000) On the equatorial Atlantic oscillation and its response to ENSO. Clim Dyn 16:213–218

Losada T, Rodriguez-Fonseca B, Polo I, Janicot S, Gervois S, Chauvin F, Ruti P (2010) Tropical response to the Atlantic Equatorial mode: AGCM multimodel approach. Clim Dyn 35:45–52. doi:10.1007/s00382-009-0624-6

Molteni F (2003) Atmospheric simulations using a GCM with simplified physical parameterizations. I- Model climatology and variability in multi-decadal experiments. Clim Dyn 20:175–191

New M, Hulme M, Jones P (1999) Representing twentieth century spacetime climate variability. Part 1: development of a 1961–1990 mean terrestrial climatology. J Clim 12:829–856

Nobre P, Shukla J (1996) Variations of sea surface temperature, wind stress, and rainfall over the tropical Atlantic and South America. J Clim 9:2464–2479

Philippon N, Doblas-Reyes FJ, Ruti PM (2010) Skill, reproducibility and potential predictability of the West African monsoon in coupled GCMs. Clim Dyn 35:53–74. doi:10.1007/s00382-010-0856-5

Rayner NA, Parker D, Horton E, Folland C, Alexander L, Rowell D, Kent E, Kaplan A (2003) Global analyses of SST, sea ice, and night marine air temperature since the late nineteenth century. J Geophys Res 108:4407. doi:10.1029/2002JD002670

Richter I, Xie SP (2008) On the origin of equatorial Atlantic biases in coupled general circulation models. Clim Dyn 31:578–598. doi:10.1007/s00,382-008-0364-z

Rodrguez-Fonseca B, Janicot S, Mohino E, Losada T, Bader J, Caminade C, Chauvin F, Fontaine B, Garca-Serrano J, Gervois S, Joly M, Polo I, Ruti P, Roucou P, Voldoire A (2010). Interannual and decadal SST-forced responses of the West African monsoon. Atmos Sci Lett. doi:10.1002/asl.308

Rodwell MJ, Hoskins BJ (2001) Subtropical anticyclones and summer monsoons. J Clim 14:3192–3211

Saravanan R, Chang P (1999) Oceanic mixed layer feedback and tropical Atlantic variability. Geophys Res Lett 26:3629–3632. doi:10.1029/1999GL010468

Saravanan R, Chang P (2000) Interaction between tropical Atlantic variability and El Niño- Southern oscillation. J Clim 13:2177–2194

Shanahan TM, Overpeck J, Anchukaitis K, Beck J, Cole J, Dettman DL, Scholz C, King J (2009) Atlantic forcing of persistent drought in West Africa. Science 324:377–380. doi:10.1126/science.1166352

Stockdale T, Balmaseda M, Vidard A (2006) Tropical Atlantic SST prediction with coupled ocean-atmosphere GCMs. J Clim 19:6047–6061

Turner A, Inness P, Slingo J (2007) The effect of doubled CO2 and model basic state biases on the monsoon-ENSO system. I- mean response and interannual variability. Q J Roy Meteor Soc 133:1143–1157. doi:10.1256/qj.82

Vizy EK, Cook K (2001) Mechanisms by which the Gulf of Guinea and eastern North Atlantic sea surface temperature anomalies can influence African rainfall. J Clim 14:795–821

Wang C, Kucharski F, Barimalala R, Bracco A (2009) Teleconnections of the Tropical Atlantic to the Tropical Indian and Pacific Oceans: a review of recent findings. Meteorol Z 18:445–454

Washington WM, Weatherly J, Meehl GAS Jr, Bettge T, CraigA WS Jr, Arblaster J, Wayland V, James R, Zhang Y (2000) Parallel climate model (PCM) control and transient simulations. Clim Dyn 16:755–774

Xi P, Arkin PA (1997) Global precipitation: a 17-year monthly analysis based on gauge observations, satellite estimates and numerical model outputs. Bull Am Meteorol Soc 78:2539–2558

Xie S, Hu K, Hafner J, Tokinaga H, Du Y, Huang G, Sampe T (2009) Indian Ocean capacitor effect on Indo-western Pacific climate during the summer following El-Niño. J Clim 22:730–747. doi:10.1175/2008JCLI2544.1

Xie P, Yatagai A, Chen M, Hayasaka T, Fukushima Y, Liu C, Yang S (2007) A gauge-based analysis of daily precipitation over East Asia. J Hydrometeor 8:607–627. doi:10.1175/JHM583.1

Xue Y, De Sales F, Lau WK-M, Boone A, Feng J, Dirmeyer P, Guo Z, Kim K-M, Kitoh A, Kumar V, Poccard-Leclercq I, Mahowald N, Moufouma-Okia W, Pegion P, Rowell DP, Schemm J, Schubert SD, Sealy A, Thiaw WM, Vintzileos A, Williams SF, Wu M-LC (2010) Intercomparison and analyses of the climatology of the West African Monsoon in the West African Monsoon modeling and evaluation project (WAMME) first model intercomparison experiment. Clim Dyn 35:3–27. doi:10.1007/s00382-010-0778-2

Yukimoto S, Noda A, Kitoh A, Sugi M, Kitamura Y, Hosaka M, Shibata K, Maeda S, Uchiyama T (2001) The new meteorological research institute coupled GCM (MRI- CGCM2)-model climate and variability. Pap Meteor Geophys 51:47–88

Zebiak S (1993) Airsea interaction in the equatorial Atlantic region. J Clim 6:1567–1586